

## Multi-band plasmonic color filters for visible-to-near-infrared image sensors

メタデータ	言語: eng 出版者: 公開日: 2018-10-19 キーワード (Ja): キーワード (En): 作成者: Miyamichi, Atsutaka, Ono, Atsushi, Kamehama, Hiroki, Kagawa, Keiichiro, Yasutomi, Keita, Kawahito, Shoji メールアドレス: 所属:
URL	<a href="http://hdl.handle.net/10297/00025821">http://hdl.handle.net/10297/00025821</a>



# Multi-band plasmonic color filters for visible-to-near-infrared image sensors

ATSUTAKA MIYAMICHI,<sup>1</sup> ATSUSHI ONO,<sup>2,\*</sup> HIROKI KAMEHAMA,<sup>1</sup>  
KEIICHIRO KAGAWA,<sup>2</sup> KEITA YASUTOMI,<sup>2</sup> AND SHOJI KAWAHITO<sup>2</sup>

<sup>1</sup>Graduate School of Science and Technology, Shizuoka University, 3-5-1 Johoku, Naka-ku, Hamamatsu 432-8561, Japan

<sup>2</sup>Research Institute of Electronics, Shizuoka University, 3-5-1 Johoku, Hamamatsu 432-8011, Japan

\*[ono.atsushi@shizuoka.ac.jp](mailto:ono.atsushi@shizuoka.ac.jp)

**Abstract:** We propose a plasmonic color filter consisting of a single aperture surrounded by concentric periodic corrugations for simultaneous imaging of a spectral range from the visible to the near-infrared. The incident light coupled with surface plasmons propagates through the sub-wavelength aperture as beaming light. The beaming light transmission is able to suppress the spatial color cross-talk between the pixels in an image sensor. We analyzed the transmission characteristics of a plasmonic color filter with periodic corrugations in a silver thin film by using the finite-difference time-domain algorithm. We demonstrated a multi-band transmission wavelength selectivity, of about 100 nm, for the spectral bandwidth ranging from visible to near-infrared. The simultaneous discrimination of visible and near-infrared light with a high color purity by the plasmonic color filter achieves both improved image recognition and smaller system-size compared with conventional systems, which is particularly important for applications such as vehicle-mounted cameras, security, and biological tissue engineering.

© 2018 Optical Society of America under the terms of the [OSA Open Access Publishing Agreement](#)

## 1. Introduction

Modern nanofabrication techniques have given rise to new color filtering techniques using subwavelength-sized metal structures for color pallets [1, 2], optical data storage [3–5], and displays [6, 7]. In particular, since color selectivity through periodic hole arrays in metallic thin films was reported by Ebbesen *et al.* in 1998 [8], color filters based on surface plasmon resonance by nanostructured metallic thin films have been actively studied for imaging applications [9–16]. Plasmonic filters made of metal are applicable to high temperature, humidity, and long-term ultraviolet exposure conditions. Metal thin films patterned with one-dimensional (1D) nano-gratings have been demonstrated to achieve spectral selectivity [10–12]. The transmission spectrum of such 1D structures depends on the polarization of the incident light, which is transmitted most efficiently when polarized perpendicular to the grating. A two-dimensional (2D) hole array in the metal thin film was proposed as another candidate design for plasmonic color filters at visible wavelengths [13, 14]. Aspects of the performance and characteristics of triangular lattice hole array filters, such as functional array size and spatial color cross-talk, has been reported [15, 16]. Plasmonic color filters have been integrated with CMOS image sensors and photodiodes to demonstrate the functionality of optical color filtering at visible wavelengths [17–20]. The wavelength filtering due to the surface plasmon resonance is determined by structural parameters such as the array period and hole diameter [8].

In this study, we focus on plasmonic color filters constructed as periodically corrugated metallic nano-gratings concentrically surrounding a single sub-wavelength aperture in front of an image sensor, as first proposed by Lezec *et al.* in 2002 [21] - the so-called “bull’s eye” structure. Recently, this type of bull’s eye plasmonic color filter has been applied to biosensing applications [22, 23]. Figure 1(a) shows a schematic of integrated plasmonic color filters with image sensors. The selected wavelength of the incident light is coupled to the surface plasmon

polaritons by corrugating the upper surfaces of the metal film. Here, the coupled surface plasmon oscillation does not couple with the lower corrugation in the metal that has a thickness of 180 nm. For metal films of this thickness, the corrugated upper and lower surfaces assume different roles in color filtering. The excited surface plasmons on the upper surface are concentrated at the center and transmitted through the sub-wavelength aperture. The transmitted photons excite surface plasmons on the lower surface. The transmitted light propagates as beaming light by coupling with the surface plasmons induced on the lower side of the corrugation. The beaming transmission is expected to be capable of suppressing spatial color cross-talk between pixels in the image sensor. The concentric corrugation proposed by Lezec is symmetric with respect to a horizontal line in the middle of metallic thin film. The film thickness is not constant, and it is required for such symmetric structure to be processed with multi-step. We found that the wavelength-selected light transmits even though the structures that are antisymmetric with respect to the horizontal line in the middle of a metallic thin film that has a constant thickness. A single-layer nanostructured metal thin film allows significant simplification of fabrication processes and device integration. The continuous corrugated nanopattern at both interfaces of the metal film is fabricated via a straightforward process of metal evaporation on the nanostructured substrate.

In conventional organic color filters, secondary transmission is generated in the near-infrared region [24]. An external infrared cut filter is typically mounted on an organic color filter to eliminate this secondary transmission of near-infrared light. In such cases, image processing systems or multispectral filter arrays are required for the simultaneous imaging of visible and near-infrared light at a single image sensor because of the external infrared cut filter [25–27]. In contrast, each color can be selected using plasmonic color filters for simultaneous imaging without an external infrared cut filter. Therefore, we propose plasmonic color filters with beaming light transmission from the visible to near-infrared band on a single sensor device for simultaneous imaging of visible and near-infrared light. Plasmonic filters can be made to form a set of bandpass filters that transmit light in different visible to near-infrared wavelength bands with a full-width at half-maximum (FWHM) of about 100 nm for each target wavelength. Plasmonic color filters with integrated image sensors can acquire visible information in addition to invisible information such as distances in time-of-flight range imaging using near-infrared light pulses [28–30]; biological imaging of the absorption of biomolecules using deep tissue penetration within the near-infrared window is also possible [31–33]. Plasmonic color filtering is expected to provide improved image recognition and reduced system size compared to conventional systems, which is

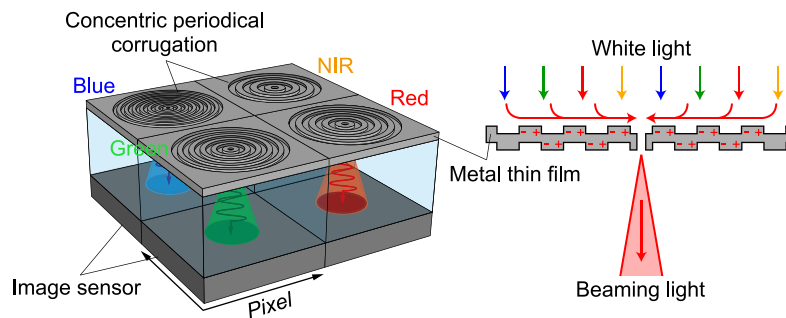


Fig. 1. Plasmonic color filters, each with a single aperture surrounded by concentric periodic corrugations. The plasmonic color filter is integrated with a single image sensor (left) for simultaneous imaging over a spectral range from the visible to near-infrared. The cross-sectional view (right) schematically illustrates the color selectivity and beaming transmission properties of a plasmonic color filter.

particularly important in applications such as vehicle-mounted cameras, security, and biological tissue engineering. Here, we design and fabricate a single-layer silver-film plasmonic filter with concentric periodic corrugations and demonstrate its wavelength selectivity in the visible to near-infrared range.

## 2. Simulation results

The transmission characteristics of a single aperture with concentric periodic grooves in a silver thin film were simulated by utilizing the finite-difference-time-domain (FDTD) algorithm, performed using commercial software FullWAVE by RSOFT. The calculation processing was simplified using a 2D simulation model of the 1D periodically corrugated silver thin film, as shown in the schematic of Fig. 2(a). Silver is suitable for surface plasmon excitation from visible to near-infrared wavelengths because it has the lowest absorption losses of all metals. The plasmonic color filter is defined by its structural parameters: the corrugation period  $p$ , groove depth  $d$ , film thickness  $t$ , and aperture diameter  $a$ . We define the simulation domain as 7 periods  $\times$  3  $\mu\text{m}$ . A non-uniform spatial grid with a combination of grid sizes gradually changing from 1 nm to 10 nm was used for the spatial grid size in both  $x$  and  $z$ -axes. A perfectly matched layer (PML) absorption boundary with a high absorption accuracy was used as the boundary conditions of the  $x$  and  $z$ -axes. The incident light was defined as an impulse wave at normal incidence with  $p$ -polarized light, which excites surface plasmons along the direction orthogonal to the corrugation period; the transmittance would be one half for unpolarized light. The transmitted wave, monitored 2  $\mu\text{m}$  below the surface of the silver thin film, was converted to a transmission spectrum via fast Fourier transformation. The transmittance was normalized by dividing the transmitted wave by the total power incident on the entire corrugated area.

The wavelength of the transmitted light that couples with the surface plasmons is mainly determined by the corrugation period because of wave vector matching with the grating vector. Figure 2(b) shows the simulated transmission spectra as a function of the corrugation period  $p$  increasing from 300 to 700 nm in 50-nm steps. The other parameters are fixed:  $t = 180$  nm,  $d = 80$  nm, and  $a = 90$  nm. When  $p = 500$  nm, the transmission at the peak wavelength of 650 nm corresponds to a transmission efficiency of 28 %. As the simulated transmission spectra in the visible to infrared region exhibit a spectral shape without secondary transmission, the proposed plasmonic filter requires no additional filters such as an infrared cut filter in order to integrate it with an image sensor. In addition, the spectral width (FWHM) at  $p = 500$  nm is about 100 nm because of the high coupling efficiency with the surface plasmon resonance, which is much narrower than the plasmonic hole array [16]. Therefore, we considered that a silver thin film with periodic corrugations, acting as an optical color filter for an image sensor, provides higher color reproducibility than previously studied plasmonic filters.

The transmittance and transmission peak wavelength also depend on parameters such as groove depth, groove width, and aperture diameter [34]. Here, we investigated the dependence of the transmission spectrum on the structural parameters of the plasmonic color filter. The peak transmission and maximum transmittance for the color red, which is designed with  $p = 500$  nm,  $d = 80$  nm,  $t = 180$  nm, and  $a = 90$  nm, are plotted as a function of the structural parameters of  $p$ ,  $d$ ,  $t$ , and  $a$  in Figs. 2(c)–2(f), respectively. We see that the peak transmission wavelength (solid line) linearly redshifts with  $p$  and  $d$  cause greater variations in peak transmittance compared with  $t$  and  $a$ . From these simulation results, we conclude that the color selectivity of the transmitted light is tuned by the corrugation period and groove depth. The film thickness and aperture diameter have optimal values for high transmittance. Figure 2(g) shows the simulation results of the transmission spectrum in the nanostructured silver film plasmonic filter optimized for blue, green, red, and near-infrared (RGB-NIR) wavelengths. Optimized structural parameters for RGB-NIR plasmonic color filters are shown in Table 1. As a result of the simulation, our plasmonic color filters exhibit a transmittance of  $\sim 30\%$  with FWHMs of their spectra of about

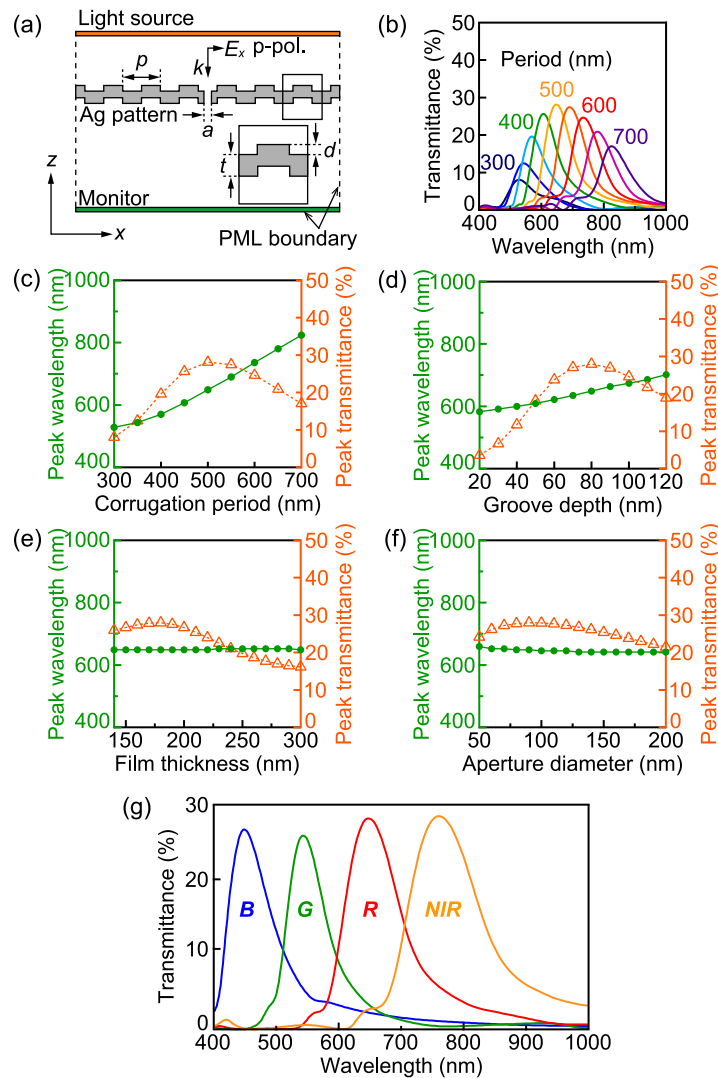


Fig. 2. Transmission characteristics of a single aperture with concentric periodic grooves in silver thin film. (a) Schematic of two-dimensional simulation model of one-dimensional periodic corrugated silver thin film. (b) Simulated transmission spectra for different values of corrugation period  $p$  between 300 and 700 nm; the other parameters are fixed as  $t = 180$  nm,  $d = 80$  nm, and  $a = 90$  nm. Peak transmission and maximum transmittance for the simulated spectra plotted as a function of the structural parameters of (c) corrugation period  $p$ , (d) groove depth  $d$ , (e) film thickness  $t$ , and (f) aperture diameter  $a$ . (g) Simulated transmission spectra of a single-layer nanostructured silver film plasmonic filter optimized for RGB-NIR wavelengths.

100 nm for each target wavelength, for normal incidence of  $p$ -polarized light. This is lower transmittance compared to commercial color filters such as dye filters or thin-film interference filters. Although there remains issues related to peak transmittance and pixel size compared to commercial color filters, simultaneous color filtering for the visible and near-infrared should be an attractive prospect for image sensor development.

We analyzed the propagation of the transmitted light of the plasmonic color filter by calculating the light intensity distribution at the peak transmission wavelength. The cross-sectional light intensity distributions in the  $x$ - $z$  plane for a corrugated lower surface structure and a flat lower

**Table 1. Optimized structural parameters\* for RGB-NIR plasmonic color filters.**

Transmission color	Corrugation period $p$	Groove depth $d$	Film thickness $t$	Aperture diameter $a$
Blue	200	30	60	60
Green	400	60	130	80
Red	500	80	180	90
Near-infrared	600	100	220	110

\*All parameter values are exhibited in units of nanometers.

surface based on the structural parameters of the red bandpass filter are shown in Figs. 3(a) and 3(b), respectively. A continuous plane wave at the peak transmission wavelength of 650 nm is irradiated from the above with normal incidence. An enhanced electric field is generated on the metal surface by resonant coupling between the incident light and surface plasmons. In the case of the corrugation of the lower surface (Fig. 3(a)), the incident light coupled with the surface plasmons is transmitted as beaming light in the normal direction through the sub-wavelength aperture. The right-hand side of intensity distribution shows the intensity line profile along the optical axis ( $a-a'$ ) at the center of the aperture. The intensity is enhanced in the aperture and the transmitted light propagates along the  $z$ -direction. The lower panel of Fig. 3(a) shows the

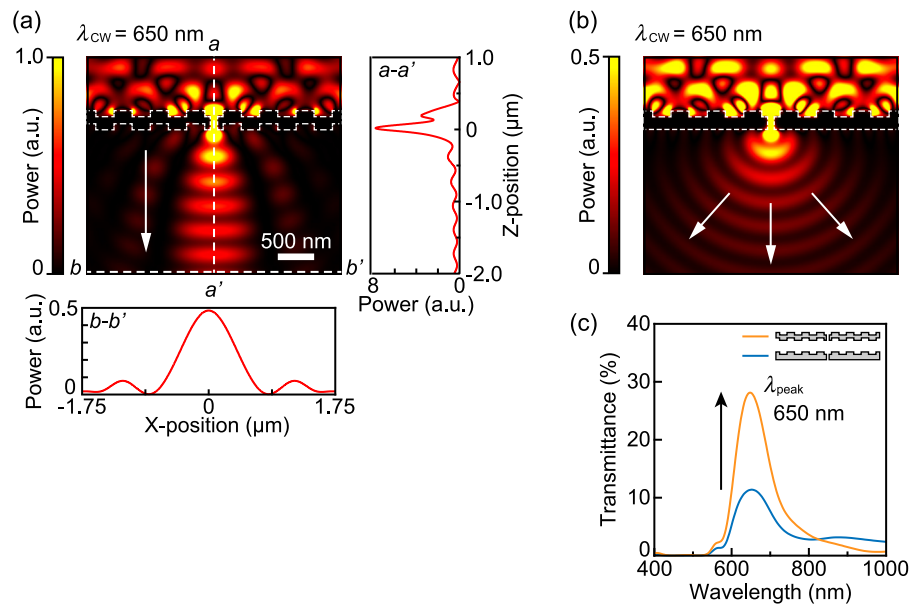


Fig. 3. (a) Spatial intensity distribution for light incidence at a peak wavelength of 650 nm for the lower corrugated surface structure of the red bandpass filter ( $p = 500$  nm,  $t = 180$  nm,  $d = 60$  nm,  $a = 90$  nm). Line profiles of intensity on the aperture center ( $a-a'$ ) and image plane ( $b-b'$ ) are plotted in the right and lower panels. Spatial intensity distribution for bottom-flat structure. For both (a) and (b), the incident continuous wave propagates vertically from top to bottom. (c) Comparison of transmission spectra of the structures with the lower corrugated surface (orange line) and flat surface (blue line).

intensity line profile along the  $x$ -axis  $2\text{-}\mu\text{m}$  below the silver thin film ( $b-b'$ ). The FWHM of the transmitted light is  $810\text{ nm}$ ; this indicates that the half-cone angle of transmitted light is  $11^\circ$ . In the case of the flat lower surface (Fig. 3(b)), transmitted light coupled with the surface plasmon propagates in all directions as a spherical distribution. It was found that the corrugation of the lower surface contributed to the beaming light transmission. We consider that this finding is essential for application of plasmonic color filters to the image sensor, suppressing the spatial color cross-talk between pixels. The comparison of the transmission spectra of the corrugated and the flat lower surfaces is shown in Fig. 3(c). The corrugation of the lower surface improved the peak transmittance by a factor of 2.5.

### 3. Experimental results

We fabricated the silver thin film of the optical color filter on a glass substrate using a standard lift-off process of electron beam lithography, vacuum evaporation, and a focused ion beam (FIB), according to the structural parameters optimized by the FDTD simulation. In this experiment, a 2D concentric periodical corrugation geometry, a rotationally symmetric structure, was fabricated for non-polarized light. A hexamethyldisilazane (HMDS) layer was spin-coated on a glass substrate to improve the adhesion of an electron beam resist layer. A ZEP520A (ZEON Corporation) positive-type electron beam resist diluted with a ZEP-A organic solvent was spin-coated and pre-baked at  $180^\circ\text{C}$  for 2 min. An Espaser conductive polymer layer was spin-coated over the resist layer to prevent charge-up. After exposure to the concentric periodic pattern with an acceleration voltage of  $80\text{ kV}$  and current of  $50\text{ pA}$ , the Espaser was removed by ultrapure water and the sample was developed in *o*-Xylene. The sample was rinsed with isopropyl alcohol and then post-baked at  $120^\circ\text{C}$  for 2 min. Silver film with a thickness of  $180\text{ nm}$  was evaporated on the patterned resist layer. Concentric corrugations were also formed on the metal surface along the resist layer pattern; thus, the groove depth  $d$  of the periodic corrugation on the front and back metal surfaces, shown in Fig. 2, is determined by the thickness of the resist layer spin-coated on the glass substrate. A sub-wavelength aperture of  $\sim 100\text{ nm}$  in diameter was drilled using a FIB with a  $30\text{-kV}$  acceleration voltage and  $10\text{-pA}$  beam current at the center of the concentric corrugation formed on the silver thin film. Figure 4(a) shows a top-view scanning electron microscope (SEM) image of the fabricated silver plasmonic color filter with  $p = 600\text{ nm}$ . Nine grooves with a period of  $600\text{ nm}$  were concentrically fabricated around the sub-wavelength aperture. Figure 4(b) shows a bird's-eye view the SEM image of Fig. 4(a). As shown in Fig. 4(b), the sub-wavelength aperture and concentric periodic corrugations were fabricated on a silver thin film. Therefore, by depositing the silver film on the patterned resist layer, the periodically corrugated metal film was easily fabricated. We fabricated plasmonic color filters with various periods from  $350$  to  $700\text{ nm}$  in  $50\text{-nm}$  steps and measured the transmission intensity distribution and spectrum.

By patterning the metal surface with a concentric periodic corrugation, the light of a selected wavelength coupled with surface plasmons can be transmitted as beaming light through the sub-wavelength aperture at the center. The transmission intensity distribution and spectrum were measured using a transmission microscope. White light from a xenon lamp was slightly focused using an objective lens with a numerical aperture of  $0.16$  and irradiated the metal surface at normal incidence. The transmitted light through the fabricated plasmonic filter was collected using an objective lens with a numerical aperture of  $0.9$  and was observed using a CCD camera. Figure 4(c) shows a bright field image observed at the transmission side of the fabricated plasmonic color filter with a groove period of  $600\text{ nm}$ . Figure 4(d) shows the transmission microscope image. A red transmission can be observed clearly from the central aperture; it is the selected wavelength corresponding to the surface plasmon coupled light.

Figure 5(a) shows the measured transmission microscope images of the plasmonic color filters with various corrugation periods in the range between  $350$  and  $700\text{ nm}$ . As shown in Fig. 5(a),

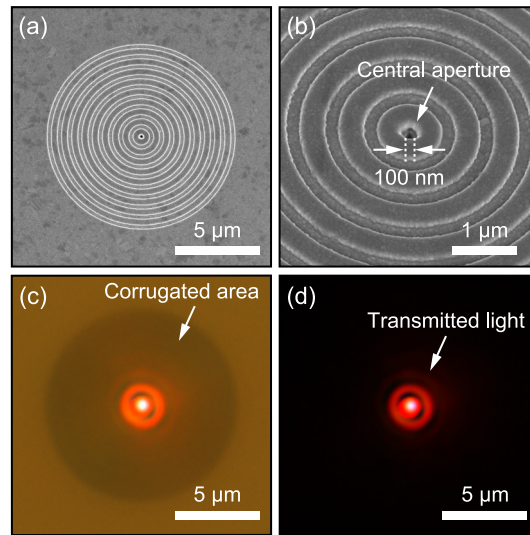


Fig. 4. SEM and optical microscope images of plasmonic color filter with concentric periodic corrugations fabricated on glass substrate ( $p = 600$  nm,  $t = 180$  nm,  $d = 80$  nm,  $a = 100$  nm). (a) Top-view SEM image of the entire plasmonic color filter corrugated with nine grooves with a period of 600 nm. (b) Bird's eye view SEM image. A sub-wavelength aperture about 100 nm in diameter is drilled at the center by FIB. (c) Bright field image observed at the transmission side of the filter. (d) Optical microscope image of the transmitted light distribution through a 180-nm-thick silver thin film. The selected red light is observed through the single sub-wavelength aperture at the center.

multiple transmitted light beams in the visible range including the three primary colors of red, green, and blue are observed in the various corrugation periods. In the spectral measurement, a multispectral transmission band with a Gaussian distribution was obtained for each plasmonic color filter, as shown in Fig. 5(b). The peak transmission wavelength shifts to longer wavelengths with increasing corrugation period. Peak transmission wavelengths corresponding to corrugation periods between 350 and 700 nm are obtained at wavelengths of 440, 475, 540, 590, 640, 680, 715, and 755 nm. The experimental transmission spectra are noisy in the near-infrared range because the spectral window of the incident light is limited to the range between 400 and 700 nm in wavelength due to an infrared cut filter inserted into the microscope to protect the objective lens from thermal damage. The actual spectral range of the plasmonic filters should extend from the ultraviolet to the infrared region, limited by the plasma frequency of the applied metal and the sensitivity range of the image sensor. Although color selectivity depending on the period is demonstrated, the peak wavelengths of the experimental spectra are shifted to shorter wavelengths, by about 100 nm, compared to those of the simulated transmission spectra shown in Fig. 2(b). The mechanism of this shift to shorter wavelengths is unclear, and further investigation is necessary to obtain good agreement between experiment and theory. The spectral bandwidth (FWHM) is about 100 nm for each plasmonic color filter. This spectral bandwidth is much narrower than that of the previously demonstrated plasmonic hole array filter.

#### 4. Conclusions

From the numerical modeling performed during this study, we obtained the optimized parameters of a plasmonic color filter with periodic corrugation of a silver thin film, leading to optical filtering functionality across the visible to near-infrared range. We successfully demonstrated the wavelength selectivity in the visible to near-infrared range of a plasmonic filter fabricated as a single-layer corrugated silver thin film. The filtering wavelength was tuned by selection of

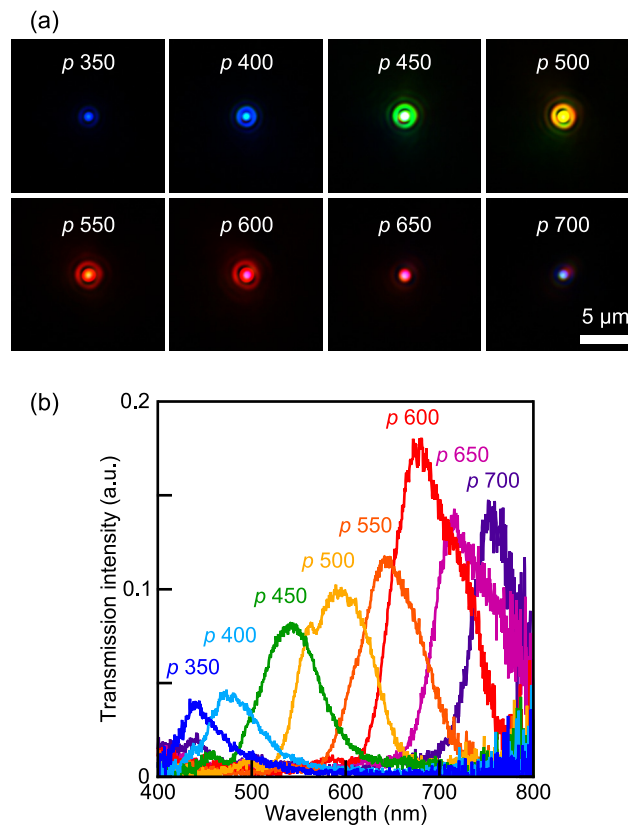


Fig. 5. Various plasmonic color filters with different corrugation periods fabricated on glass substrate. (a) Optical microscope images of plasmonic color filter with corrugation period ranging from 350 to 700 nm. Multicolor transmission is observed with the set of filters. (b) Measured transmission spectra for each filter shown in (a). Multi-band spectra with a bandwidth of approximately 100 nm appear in the visible to near-infrared range.

an appropriate corrugation period. A multispectral band with an FWHM of about 100 nm was demonstrated for each plasmonic filter; although it should be noted that the spectral bandwidth will be slightly broader for typical optical sensor incident angles of 10-20 degree than that obtained at normal incidence. A simulation using 2D model was applied to understand of the basic color filtering characteristics of the arrangement. Further analysis using a 3D model would be required to show good agreement between experiment and simulation. We applied a FIB milling technique for fabrication of the 100-nm sized aperture; however, this technique is for prototyping, and is not well-suited for mass production. It remains one of the significant issues for manufacturing image sensors add-on our proposed plasmonic filter to consider the mass production process.

Silver is suitable for simultaneous imaging using visible and near-infrared signals because of the high coupling efficiency due to the lowest absorption losses of metals across the visible to near-infrared waveband. In this paper, we chose to use silver as the plasmonic material for this reason. However, we need to consider possible damage by oxidation or the aging in the context of practical applications. Although gold is a chemically stable material, it cannot obtain a plasmon resonance in the blue wavelengths due to the plasma frequency around 500 nm. Gold is, however, desirable for filtering applications in the near-infrared to infrared wavelength region. In the case of aluminum, absorption losses are higher than for silver, but its use allows a larger waveband

from the deep ultraviolet to the infrared, to be detected; in addition, aluminum is compatible with the standard CMOS process.

In summary, plasmonic color filtering will lead to the realization of multispectral imaging devices, and it is expected to provide improved image recognition and reduce the system size of conventional image sensors. Further, we believe that our plasmonic color filter for simultaneous imaging will facilitate new discoveries in the fields of biophotonics, opto-electronics, and plasmonics research.

## Funding

Japan Society for the Promotion of Science (JSPS) KAKENHI Grant-in-Aid for Scientific Research on Innovative Areas [Grant nos. 16H00947, 26109505].

## References

1. K. Kumar, H. Duan, R. S. Hegde, S. C. W. Koh, J. N. Wei, and J. K. W. Yang, "Printing colour at the optical diffraction limit," *Nat. Nanotechnol.* **7**, 557–561 (2012).
2. S. J. Tan, L. Zhang, D. Zhu, X. M. Goh, Y. M. Wang, K. Kumar, C.-W. Qiu, and J. K. W. Yang, "Plasmonic color palettes for photorealistic printing with aluminum nanostructures," *Nano Lett.* **14**, 4023–4029 (2014).
3. E. Heydari, J. R. Sperling, S. L. Neale, and A. W. Clark, "Plasmonic color filters as dual-state nanopixels for high-density microimage encoding," *Adv. Funct. Mater.* **27**, 1616–3028 (2017).
4. T. Chen and B. M. Reinhard, "Assembling color on the nanoscale: Multichromatic switchable pixels from plasmonic atoms and molecules," *Adv. Mater.* **28**, 3522–3527 (2016).
5. Y.-W. Huang, W. T. Chen, W.-Y. Tsai, P. C. Wu, C.-M. Wang, G. Sun, and D. P. Tsai, "Aluminum plasmonic multicolor meta-hologram," *Nano Lett.* **15**, 3122–3127 (2015).
6. C. Williams, G. Rughoobur, A. J. Flewitt, and T. D. Wilkinson, "Nanostructured plasmonic metapixels," *Sci. Rep.* **7**, 7745 (2017).
7. J. Olson, A. Manjavacas, L. Liu, W.-S. Chang, B. Foerster, N. S. King, M. W. Knight, P. Nordlander, N. J. Halas, and S. Link, "Vivid, full-color aluminum plasmonic pixels," *PNAS* **111**, 14348–14353 (2014).
8. T. W. Ebbesen, H. J. Lezec, H. F. Ghaemi, T. Thio, and P. A. Wolff, "Extraordinary optical transmission through sub-wavelength hole arrays," *Nature* **391**, 667–669 (1998).
9. L. Frey, P. Parrein, J. Raby, C. Pell'Ät, D. HÄlfrault, M. Marty, and J. Michailos, "Color filters including infrared cut-off integrated on cmos image sensor," *Opt. Express* **19**, 13073–13080 (2011).
10. P. B. Catrysse and B. A. Wandell, "Integrated color pixels in 0.18-Åm complementary metal oxide semiconductor technology," *J. Opt. Soc. Am. A* **20**, 2293–2306 (2003).
11. B. Zeng, Y. Gao, and F. J. Bartoli, "Ultrathin nanostructured metals for highly transmissive plasmonic subtractive color filters," *Sci. Rep.* **3**, 2840 (2013).
12. E. Laux, C. Genet, T. Skauli, and T. W. Ebbesen, "Plasmonic photon sorters for spectral and polarimetric imaging," *Nat. Photonics* **2**, 161–164 (2008).
13. H.-S. Lee, Y.-T. Yoon, S.-S. Lee, S.-H. Kim, and K.-D. Lee, "Color filter based on a subwavelength patterned metal grating," *Opt. Express* **15**, 15457–15463 (2007).
14. Q. Chen and D. R. S. Cumming, "High transmission and low color cross-talk plasmonic color filters using triangular-lattice hole arrays in aluminum films," *Opt. Express* **18**, 14056–14062 (2010).
15. R. Rajasekharan, E. Balaur, A. Minovich, S. Collins, T. D. James, A. Djalalian-Assl, K. Ganesan, S. Tomljenovic-Hanic, S. Kandasamy, E. Skafidas, D. N. Neshev, P. Mulvaney, A. Roberts, and S. Praver, "Filling schemes at submicron scale: Development of submicron sized plasmonic colour filters," *Sci. Rep.* **4**, 6435 (2014).
16. S. Yokogawa, S. P. Burgos, and H. A. Atwater, "Plasmonic color filters for cmos image sensor applications," *Nano Lett.* **12**, 4349–4354 (2012).
17. Q. Chen, D. Chitnis, K. Walls, T. D. Drysdale, S. Collins, and D. R. S. Cumming, "Cmos photodetectors integrated with plasmonic color filters," *IEEE Photon. Tech. L.* **24**, 197–199 (2012).
18. Q. Chen, D. Das, D. Chitnis, K. Walls, T. D. Drysdale, S. Collins, and D. R. S. Cumming, "A cmos image sensor integrated with plasmonic colour filters," *Plasmonics* **7**, 695–699 (2012).
19. S. P. Burgos, S. Yokogawa, and H. A. Atwater, "Color imaging via nearest neighbor hole coupling in plasmonic color filters integrated onto a complementary metal-oxide semiconductor image sensor," *ACS Nano* **7**, 10038–10047 (2013).
20. B. Y. Zheng, Y. Wang, P. Nordlander, and N. J. Halas, "Color-selective and cmos-compatible photodetection based on aluminum plasmonics," *Adv. Mater.* **26**, 6318–6323 (2014).
21. H. J. Lezec, A. Degiron, E. Devaux, R. A. Linke, L. Martin-Moreno, F. J. Garcia-Vidal, and T. W. Ebbesen, "Beaming light from a subwavelength aperture," *Science* **297**, 820–822 (2002).
22. C. R. Crick, P. Albella, H.-J. Kim, A. P. Ivanov, K.-B. Kim, S. A. Maier, and J. B. Edel, "Low-noise plasmonic nanopore biosensors for single molecule detection at elevated temperatures," *ACS Photonics* **4**, 2835–2842 (2017).

23. C. R. Crick, P. Albella, B. Ng, A. P. Ivanov, T. Roschuk, M. P. Cecchini, F. Bresme, S. A. Maier, and J. B. Edel, "Precise attoliter temperature control of nanopore sensors using a nanoplasmonic bullseye," *Nano Lett.* **15**, 553–559 (2015).
24. Z. Chen, X. Wang, and R. Liang, "Rgb-nir multispectral camera," *Opt. Express* **22**, 4985–4994 (2014).
25. C. Park and M. G. Kang, "Color restoration of rgbn multispectral filter array sensor images based on spectral decomposition," *Sensors* **16**, 719 (2016).
26. H. Tang, X. Zhang, S. Zhuo, F. Chen, K. N. Kutulakos, and L. Shen, "High resolution photography with an rgb-infrared camera," in *Proceedings of 2015 IEEE International Conference on Computational Photography*, (IEEE, 2015), pp. 1–10.
27. P. J. Lapray, X. Wang, J. B. Thomas, and P. Gouton, "Multispectral filter arrays: recent advances and practical implementation," *Sensors* **14**, 21626–21659 (2014).
28. R. Lange and P. Seitz, "Solid-state time-of-flight range camera," *IEEE J. Quantum Elect.* **37**, 390–397 (2001).
29. S. Kawahito, I. A. Halin, T. Ushinaga, T. Sawada, M. Homma, and Y. Maeda, "A cmos time-of-flight range image sensor with gates-on-field-oxide structure," *IEEE Sens. J.* **7**, 1578–1586 (2007).
30. S.-M. Han, T. Takasawa, K. Yasutomi, S. Aoyama, K. Kagawa, and S. Kawahito, "A time-of-flight range image sensor with background canceling lock-in pixels based on lateral electric field charge modulation," *IEEE J. Electron Devices Soc.* **3**, 267–275 (2015).
31. R. R. Anderson and J. A. Parrish, "The optics of human skin," *J. Invest. Dermatol.* **77**, 13–19 (1981).
32. J. V. Frangioni, "In vivo near-infrared fluorescence imaging," *Curr. Opin. Chem. Biol.* **7**, 626–634 (2003).
33. E. A. Owens, M. Henary, G. E. Fakhri, and H. S. Choi, "Tissue-specific near-infrared fluorescence imaging," *Acc. Chem. Res.* **49**, 1731–1740 (2016).
34. O. Mahboub, S. C. Palacios, C. Genet, F. J. Garcia-Vidal, S. G. Rodrigo, L. Martin-Moreno, and T. W. Ebbesen, "Optimization of bull's eye structures for transmission enhancement," *Opt. Express* **18**, 11292–11299 (2010).